Technical University of Denmark

3D Lagrangian VPM: simulations of the near-wake of an actuator disc and horizontal axis wind turbine

Berdowski, T.; Ferreira, Célia Maria Dias; Walther, Jens Honore

Link back to DTU Orbit

DTU Library
Technical Information Center of Denmark

3D Lagrangian VPM: simulations of the near-wake of an actuator disc and horizontal axis wind turbine

T Berdowski[1]**, C Ferreira**[1]**, J Walther**[2]

(1) Delft University of Technology, Kluyverweg 1, 2629HS Delft, The Netherlands.
(2) Technical University of Denmark, Anker Engelunds Vej 1 Bygning 101A, 2800 Kgs. Lyngby, Denmark.

E-mail: `T.J.Berdowski@tudelft.nl`

Abstract. The application of a 3-dimensional Lagrangian vortex particle method has been assessed for modelling the near-wake of an axisymmetrical actuator disc and 3-bladed horizontal axis wind turbine with prescribed circulation from the MEXICO (Model EXperiments In COntrolled conditions) experiment. The method was developed in the framework of the open-source Parallel Particle-Mesh library for handling the efficient data-parallelism on a CPU (Central Processing Unit) cluster, and utilized a $\mathcal{O}(N \log N)$-type fast multipole method for computational acceleration. Simulations with the actuator disc resulted in a wake expansion, velocity deficit profile, and induction factor that showed a close agreement with theoretical, numerical, and experimental results from literature. Also the shear layer expansion was present; the Kelvin-Helmholtz instability in the shear layer was triggered due to the round-off limitations of a numerical method, but this instability was delayed to beyond 1 diameter downstream due to the particle smoothing. Simulations with the 3-bladed turbine demonstrated that a purely 3-dimensional flow representation is challenging to model with particles. The manifestation of local complex flow structures of highly stretched vortices made the simulation unstable, but this was successfully counteracted by the application of a particle strength exchange scheme. The axial and radial velocity profile over the near wake have been compared to that of the original MEXICO experiment, which showed close agreement between results.

1. Introduction

The Blade Element Momentum (BEM) theory has traditionally formed the core of aerodynamic design applications in the wind energy industry [1]. BEM models have proved to be both fast and accurate for many operational design conditions of the traditional Horizontal Axis Wind Turbine (HAWT), but the 2D blade assumption and implicit wake modelling also pose its limits. This is especially true in case of unsteady wake phenomena, such as with yawed or sheared flow, dynamic inflow, wake meandering, wake-blade interactions, etc.

In the present paper, the application of a Vortex Particle Method (VPM) is considered for the explicit modelling of the near-wake of a HAWT machine. A VPM relies on a description of the Navier-Stokes equations in vorticity form, and a discretization of the vorticity field by freely convecting particle sources. Such a mesh-free or Lagrangian method offers some interesting advantages over classical Computational Fluid Dynamics (CFD) approaches of which the most important one is probably its auto-adaptivity: the flow is only modelled at regions of concentrated vorticity, infinite boundary conditions are implicitly accounted for, and there is no need of an explicit modelling of refined grid structures as there is no grid. Other

advantages include the absence of numerical diffusion, the Courant-Friedrichs-Lewy (CFL) condition, and the pressure term (which is now implicitly described through vorticity instead). This makes a VPM especially well-suited for problems involving unsteady high-Reynolds flows with concentrated flow complexities, such as bluff body flows and in our case the wake of a wind turbine.

VPMs have been applied in the wind energy sector, but implementations often rely on a particle-mesh description. Particles are advected in a Lagrangian manner, but the mesh then allows for the the convenient treatment of differential operators, grid distortion corrections, and computational acceleration through the use of fast Poisson solvers. Chatelain et al. [2] developed such a method coupled to a Large Eddy Simulation (LES) to model the unsteady, turbulent flow to study the wake meandering of two turbines in tandem. Later, this model was applied to assess the large-scale wake of the Tjæreborg turbine [3]. In the 1990s, Voutsinas [4] developed GENUVP (GENeral Unsteady Vortex Particle code), which is a 3D panel code with a Lagrangian wake description through vortex particles, and applied it to model the wake of wind turbines in yawed conditions. More often, the use of VPMs arise in other fields of science. Yokota et al. [5, 6, 7, 8] have applied a Fast Multipole Method (FMM) based Lagrangian VPM on a GPU (Graphics Processing Unit) cluster for the simulation of isotropic turbulence. Hu et al. [9, 10] have applied a similar method for the computation of helicopter wakes for specific operational modes.

With the current work it is aimed to identify opportunities and issues involved in modelling the 3-dimensional near-wake of a HAWT with a VPM. It is strived for to maintain the Lagrangian particle description to exploit the benefits of auto-adaptivity. The VPM is written in *Fortran* [11], and applies the open-source Parallel Particle-Mesh (PPM) library [12] for handling the data-parallelism on a CPU (Central Processing Unit) cluster. A coupling to a FMM allows for computational acceleration beyond domain sizes of a few thousand particles. With the VPM, the near-wake of both an Actuator Disc (AD) and a 3-bladed HAWT with prescribed circulation are investigated, to assess the numerical accuracy, convergence, stability, and efficiency properties of such a flow described by discretized particles.

2. Vortex Particle Method
In the following subsections a basic introduction into the concept of the VPM is given, based on the textbook of Cottet and Koumoutsakos [13] and the dissertation of Winckelmans [14]. The reader is referred to these works for a more in depth coverage of the topic.

2.1. Fundamental equations of a vortex method
The Navier-Stokes equations in vector notation for an incompressible fluid, and void of any external forces and buoyancy effects, is described by equation 1. p, ρ, and ν are the pressure, density, and kinematic viscosity respectively.

$$\frac{D\vec{u}}{Dt} = \frac{d\vec{u}}{dt} + \vec{u} \cdot \nabla \vec{u} = -\nabla \frac{p}{\rho} + \nu \nabla^2 \vec{u} \tag{1}$$

We can introduce a quantity called vorticity, which is defined as the curl of the velocity, see equation 2. With this quantity, equation 1 can be rewritten in a concise format without an explicit need of computing the pressure term p and infinite boundary conditions . If we take the curl of equation 1 and apply the vector identity $\vec{u} \cdot \nabla \vec{u} = \frac{1}{2}\nabla \vec{u}^2 - \vec{u} \times \vec{\omega}$, equation 3 is obtained. Note that the striked through term containing the pressure disappears due to another vector identity $\nabla \times (\nabla \phi) = 0$, with ϕ being any scalar.

$$\vec{\omega} \equiv \nabla \times \vec{u} \tag{2}$$

$$\nabla \times \frac{d\vec{u}}{dt} = \frac{d\vec{\omega}}{dt} = \nabla \times (\vec{u} \times \vec{\omega}) - \nabla \times \frac{1}{\rho}\nabla\left(p + \frac{1}{2}\rho\vec{u}^2\right) + \nu\nabla^2\vec{\omega} \tag{3}$$

A further simplification of equation 3 can be obtained by considering the identity of equation 4. An incompressible fluid is divergence-free, meaning that the last two terms of this identity drop out. This results in the vorticity transport equation (equation 5, which describes the time evolution of vorticity in a Lagrangian framework.

$$\nabla \times (\vec{u} \times \vec{\omega}) = \vec{\omega} \cdot \nabla\vec{u} - \vec{u} \cdot \nabla\vec{\omega} + \vec{u}(\nabla \cdot \vec{\omega}) - \vec{\omega}(\nabla \cdot \vec{u}) \tag{4}$$

$$\frac{D\vec{\omega}}{Dt} \equiv \frac{d\vec{\omega}}{dt} + \vec{u} \cdot \nabla\vec{\omega} = \underbrace{\vec{\omega} \cdot \nabla\vec{u}}_{\text{convection}} + \underbrace{\nu\nabla^2\vec{\omega}}_{\text{diffusion}} \tag{5}$$

The convective term is often rewritten as the product of a Jacobian matrix of the velocity gradient with the vorticity: $\vec{\omega} \cdot \nabla\vec{u} = [\nabla\vec{u}]\,\vec{\omega}$. The vorticity transport equation, together with the relationship between vorticity and velocity (equation 2), form the fundamental descriptions of a vortex method. As the vorticity itself is a solution to a certain streamfunction ($\nabla^2\vec{\psi} = -\vec{\omega}$) due to the incompressibility assumption and the velocity is the curl of this streamfunction ($\vec{u} = \nabla \times \vec{\psi}$), equation 2 can be inverted and solved by applying a convolution with the Green's function for a Laplace equation, see equation 6.

$$\vec{u} = \nabla \times \vec{\psi} = \nabla \times (G * \vec{\omega}) \tag{6}$$

2.2. Discretization of the continuum fluid by particle elements
The expressions for a continuum fluid can be discretised using singular particle sources (referred to with the super-index p or q in this paper) which carry a vector strength $\vec{\alpha}^p$ and convect with the flow as were it material points. These particle strengths are defined as the domain integral over an element of vorticity (for instance discrete vortex line segments): $\vec{\alpha}^p = \int_D \vec{\omega}^p dD$. Equation 6 is then rewritten in a discrete sense as a summation over all the particles in the domain, see equation 7. $\vec{K}$ is the Biot-Savart kernel and it is defined as the gradient of the Green's function of the Laplace equation (equation 8).

$$\vec{u}(\vec{x}) = \nabla \times (G(\vec{x}) * \vec{\omega}(\vec{x})) \approx \sum_q \nabla G(\vec{x} - \vec{x}^q) \times \vec{\alpha}^q = \sum_q \vec{K}(\vec{x} - \vec{x}^q) \times \vec{\alpha}^q \tag{7}$$

$$\vec{K} \equiv \nabla G = \nabla\left(\frac{-1}{4\pi r}\right) = \frac{-\vec{r}}{4\pi r^3} \tag{8}$$

As the Biot-Savart kernel is singular, a smoothing has to be applied at least for near-field interactions. This is done by introducing a cut-off function $g(\rho)$, and implementing it into the Biot-Savart kernel: $\vec{K}_\sigma = g(\rho)\frac{\vec{r}}{r^3}$. A normalized radius $\rho = r/\sigma$ has been introduced, with σ being the characteristic smoothing radius of the particle. Such a smoothing is referred to as regularization of the singular particle field.

Also the vorticity transport equation has to be discretised. Assuming inviscid flow, a regularized expression of the vortex stretching is given in equation 9. Another form of this expression can be obtained by taking the transpose of the velocity Jacobian: $[\nabla\vec{u}]^T$, see equation 10. This equation is called the transpose form of the vortex stretching, while equation 9 is then referred to as the classic form. Both expressions are equal in the continuum case of incompressible flows, as: $[\nabla\vec{u}]\,\vec{\omega} = [\nabla\vec{u}]^T\vec{\omega}$. In the discrete sense, the divergence-free condition is only approximated (the striped through terms of equation 4 do not drop out), such that the convergence and stability properties of both expressions generally differ.

$$\frac{D\vec{\alpha}^p}{Dt} = -\sum_q \left(\frac{1}{\sigma^3} \frac{g(\rho)}{\rho^3} \vec{\alpha}^p \times \vec{\alpha}^q + \frac{1}{\sigma^5 \rho} \frac{d}{d\rho} \left(\frac{g(\rho)}{\rho^3} \right) (\vec{\alpha}^p \cdot \vec{r}) (\vec{r} \times \vec{\alpha}^q) \right) \tag{9}$$

$$\frac{D\vec{\alpha}^p}{Dt} = \sum_q \left(\frac{1}{\sigma^3} \frac{g(\rho)}{\rho^3} \vec{\alpha}^p \times \vec{\alpha}^q + \frac{1}{\sigma^5 \rho} \frac{d}{d\rho} \left(\frac{g(\rho)}{\rho^3} \right) (\vec{\alpha}^p \cdot (\vec{r} \times \vec{\alpha}^q)) \cdot \vec{r} \right) \tag{10}$$

2.3. Viscous diffusion term

A vortex method is especially suited for the treatment of unsteady, incompressible, high-Reynolds flows, but also for turbulent flows the treatment of viscous diffusion is of great importance. As time passes, the cascade of turbulence will eventually result in the occurrence of very small energy scales consisting of prohibitively intense vortices [13]. If the vorticity is not dissipated from these highly stretched vortex regions, the numerical simulation will soon enough become unstable.

Several methods for viscous diffusion have been proposed over the years which respect the Lagrangian nature of a vortex method. Often this involves the strategy of viscous-splitting as formulated by Chorin [15], with which the convective and diffusive terms are solved in consecutive substeps. In the same paper he introduced the well-known random-walk method, which mimics diffusion by updating the particle locations in a stochastic manner. However, the random-walk method is too inaccurate for lower Reynolds simulations. Due to its simplicity, the core spreading method is another often applied approach [16]. This method also involves viscous-splitting, but instead of updating particle positions, diffusion is modelled by letting the core grow over time. As the core grows beyond the characteristic length scales over time, a corrected core spreading method was introduced, whereby the particles are split into smaller particles which are redistributed in radial direction [17].

For the present work, a method is implemented which relies on distribution of the particle strengths instead, known as the Particle Strength Exchange (PSE) scheme [18]. It has some advantages over other methods: viscous splitting is not required, it is more accurate for lower Reynolds numbers, and splitting into smaller particles over time is not required which could otherwise prove to be computationally expensive. However, the method is of cost $\mathcal{O}(N^2)$ and requires the tracking of the particle volumes. The general expression for the diffusive term of the particle strength evolution using a PSE scheme is presented in equation 11. As the influence of particles decays with $\mathcal{O}(r^{-5})$ one can adopt a strategy of neglecting far-field interactions to relax the computational effort of this scheme.

$$\frac{D\vec{\alpha}^p}{Dt} = \sum_q \frac{\nu}{\sigma^5} \left(\frac{4}{\rho^4} \frac{dg(\rho)}{d\rho} - \frac{2}{\rho^3} \frac{d^2 g(\rho)}{d\rho^2} \right) (vol^p \vec{\alpha}^q - vol^q \vec{\alpha}^p) \tag{11}$$

2.4. Lagrangian grid distortions and particle divergence

As time passes by the flow strain will locally result in the accumulation of particles and on the other hand also in regions void of any particles. Although usually no error is manifested in the global quantities (linear, angular impulse, etc.), locally the vortex geometries get distorted. These grid distortions are related to the amount of flow strain present and are a result of the numerical truncation errors which exponentially amplify over time [13]. For the current method, grid distortions are not actively corrected. An exception involves the relaxation of divergence by a filtering mechanism as proposed by Predrizzetti [19]. It is applied for cases involving the transposed stretching scheme, as opposed to the classic scheme it does not inherently conserve the solenoidal flow conditions in regions of high flow strain. The algorithm works by correcting the particle strength according to a small filter f, see equation 12.

$$\vec{\alpha}^p_{\text{new}} = (1 - f\Delta t)\,\vec{\alpha}^p_{\text{old}} + f\Delta t\,\frac{\vec{\omega}_\sigma(\vec{x}^p)}{\|\vec{\omega}_\sigma(\vec{x}^p)\|}\,\big\|\vec{\alpha}^p_{\text{old}}\big\| \tag{12}$$

2.5. Computational acceleration

As the computational cost of an N-body problem scales with $\mathcal{O}(N^2)$, both the parallelisation and the application of hierarchical acceleration algorithms are a necessity for particle-based methods. Two types of hierarchical methods are in common use [7], whereby the treecode [20] is traditionally in use by the astrophysics community, while vortex methods for continuum fluids rely often on Fast Multipole Methods (FMM) [21]. The treecode can optimally provide a computational scaling to $\mathcal{O}(N \log N)$, while (depending on the implementation type) $\mathcal{O}(N \log N)$ or even $\mathcal{O}(N)$ are theoretically obtainable with an FMM. Since the advent of the CUDA (Compute Unified Device Architecture) programming environment in 2006 [9], the implementation of hierarchical algorithms on GPU clusters has gained popularity. However, the obtainable speed-up for the treecode and FMM on the GPU has lacked that of direct computations due to the low data-parallelism of the multipole moments in the box structure [7]. The current method relies on a parallelization on the CPU instead, and on the application of an $\mathcal{O}(N \log N)$-type FMM.

2.6. Description of the numerical implementation

A VPM has been developed in *Fortran* and able to run in parallel on a cluster of CPUs. For the parallel data handling, the VPM relies on the open-source Parallel Particle Mesh (PPM) library [12] built on the Message Passing Interface (MPI) standard. For further acceleration, an $\mathcal{O}(N \log N)$-type CPU-based FMM is implemented following the description by Greengard [21], which is an extension of the PPM library. The FMM in its original formulation provided only the potential or streamfunction of the Coulomb kernel, such that it had to be rewritten for this project for the acquisition of the Biot-Savart kernel and vortex stretching terms [22].

The vorticity field is described by either singular or regularized particles (Gaussian and low- or high-order algebraic), and time integration follows a Eulerian, 2nd order Runge-Kutta, or 4th order Runge-Kutta scheme. Vortex stretching is handled by the classic, transposed, or a mixed scheme, whereby particles are split during stretching to guarantee core overlap. A filtering algorithm by Pedrizzetti may be applied to relax vorticity divergence. Viscous diffusion can be modelled through a core growth model or PSE scheme.

3. Simulation setup

In this paper, two cases will be discussed that are simulated with the VPM code. The first case involves an axisymmetrical AD, while a second case with a 3-bladed HAWT applied provides a challenging modelling case as the simulation is now truly 3-dimensional. The AD simulations were run for a few hours each on an Intel Core i7-3537U CPU with a basic clock speed of 2.0 GHz. The simulations with the 3-bladed turbine have been given 240 hours of run time each on a single Intel Xeon CPU E5-2670v2 with a clock speed of 2.5 GHz, whereby the FMM was applied with an expansion order of $p = 2$ and an acceptance factor of $\theta = 2.0$.

3.1. Axisymmetrical Actuator Disc

The first case that is run is that of an axisymmetrical Actuator Disc (AD) of radius $R/D = 0.5$ whereby vortex rings are shed which are discretized through regularized particles to provide a core overlap at initiation (figure 1, left frame). $N = 50$ particles make up each ring, with a relatively large core size of $\sigma/D = 0.1$, whereby an initial particle strength according to equation 13 is given (with C_T the thrust coefficient of the AD and u_∞ the freestream velocity). A time

step of $\Delta t = 0.025[s]$ and run time of $t = 75[s]$ result in the total shedding of 3000 vortex rings. A 2nd order Runge-Kutta scheme is applied.

$$\|\vec{\alpha}^p\| = \frac{\pi R}{N} C_T u_\infty^2 \Delta t \tag{13}$$

For computational relaxation, use is made of the axisymmetry whereby the influence of the vorticity field is only calculated on one particle per ring. The result is then translated to the other particles on the ring. The far-wake from 5 diameters downstream and beyond is replaced by an analytical description of a semi-infinite vortex tube [23]. Fore more background information on the analytical description of an actuator disc, the reader is referred to for instance the work of Yu et al. [24].

3.2. 3-bladed HAWT with prescribed circulation
The second case involves a rotating 3-bladed HAWT machine, whereby the circulation over the blade span is prescribed and kept constant (figure 1, right frame). The blade circulation distribution is obtained empirically from the MEXICO (Model rotor EXperIments under COntrolled conditions) experiment at a tip speed ratio of $TSR = 6.67$ and a chordwise Reynolds number at 75% blade span of $Re = 6 \cdot 10^5$ [25, 26]. For the simulations the rotor radius R is scaled to unity with a maximum chord radius of $c_{\max} = 0.107[m]$. A free-stream velocity of $u_\infty = 0.942[m/s]$ is applied, such that each second the rotor makes exactly one full rotation (i.e. $t = 1[s]$ corresponds to $NR = 1$, with NR being the Number of Rotations). The time step is set to $\Delta t = 0.05[s]$ and the runtime is in the order of $NR = 5$ to about $NR = 15$. Each time step, particles were shed from 9 radial positions over the blade, with a constant core size of $\sigma = 0.1[m]$. Particle splitting was applied to maintain a core overlap of $\sigma/h \geq 1.5$, with h the inter-particle distance between core centers.
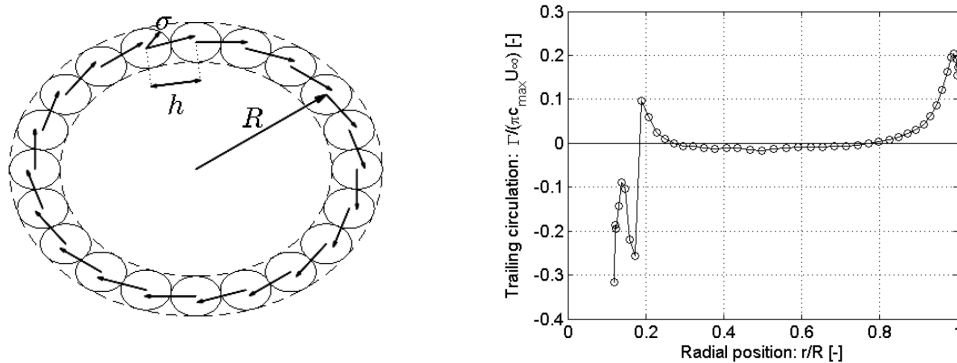
Figure 1. Vortex rings discretization by particles for the AD (left), and circulation distribution over the blade from the MEXICO experiment (right).

4. Results and discussions of simulations utilizing an Actuator Disc
4.1. Visualizing the wake and Kelvin-Helmholtz instability with particles
To give an insight into the behaviour of the particles after initiation at the disc edges, figure 2 is constructed. The top frame shows the axial velocity profile over the wake for a simulation at the Betz limit ($C_T = 0.89$), with the particles visualized through a collection of black dots in the shear layer. As the simulation is symmetric, only the top half of the wake is shown, with the AD present as a vertical solid black line. The semi-infinite analytical vortex tube representation is apparent from 5 diameters downstream onwards by a dashed box. A close-up of this wake is

presented in the bottom frame, where the vorticity resulting from the smooth particle field is shown.

It is visible that the wake starts expanding aft of the AD. After 1 diameter downstream, the shear layer becomes unstable due to the numerical limits involving round-off errors of the floating-point approximation. At 1.5 diameters downstream the formation of a typical Rosenhead vortex is distinguishable which soon breaks up to form clouds of particles which start to rotate around each other (leapfrogging). This phenomenon is a clear example of the Kelvin-Helmholtz instability, and as a result the shear layer starts expanding. Another consequence is that the theoretical wake expansion ($D_{\text{far-wake}}/D_{\text{AD}} = \sqrt{2}$) is not achieved. The semi-infinite analytical vortex tube then forces the under-expanded wake to collapse to some extent, and the axial induction between 4 and 5 diameters downstream is therefore over-predicted.
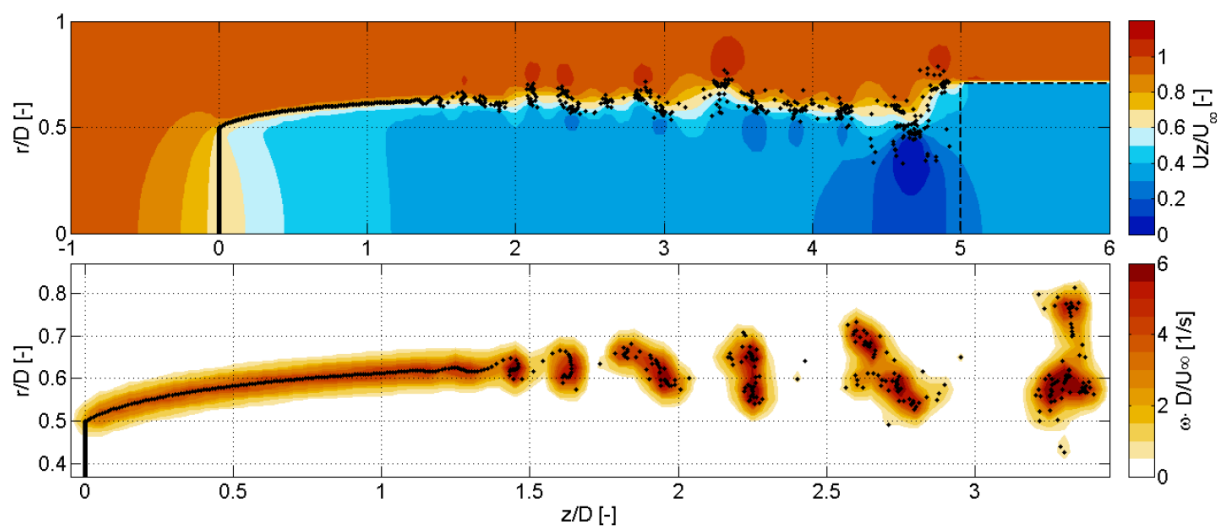
Figure 2. Visualization of the instantaneous axial velocity profile in the near-wake of an AD by particles (top), and a close-up of the vorticity in the shear-layer showing the Kelvin-Helmholtz instability and leapfrogging event (bottom).

4.2. Comparison of the axial velocity with a PIV experiment
In figure 3 the average axial velocity in the near-wake obtained with a simulation of the AD at the Betz limit ($C_T = 0.89$) (top figure) is compared to that of a Particle Image Velocimetry (PIV) experiment from literature at a marginally higher thrust coefficient of $C_T = 0.93$ [27]. Note that with the experiment no results have been obtained for the blank region due to limitations in the PIV setup. When the raw data of the PIV experiment was originally received, it was understood that this was for $C_T = 0.89$. It was only realized after running the simulation campaign that the comparison material was run at a somewhat higher $C_T = 0.93$, explaining the choice for a different thrust coefficient.

The simulation and experiment show a comparable behaviour in wake expansion and shear layer expansion, but the onset of shear layer expansion takes place at different positions. Due to the regularized particles, the shear layer of the simulation is smooth right from the initialization and starts expanding after about 1 diameter downstream due to the Kelvin-Helmholtz instability (as visualized in figure 2). The shear layer in the experiment is sharp at the onset and therefore starts expanding right away. This results in a somewhat larger expansion beyond 2 diameters downstream for the experiment. The wake itself is smooth for the simulation, while the experiment shows a more differentiated profile due to the presence of a physical, perforated

actuator disc. Finally, there is a small difference in wake deficit as a slightly higher thrust coefficient has been applied for the experiment.
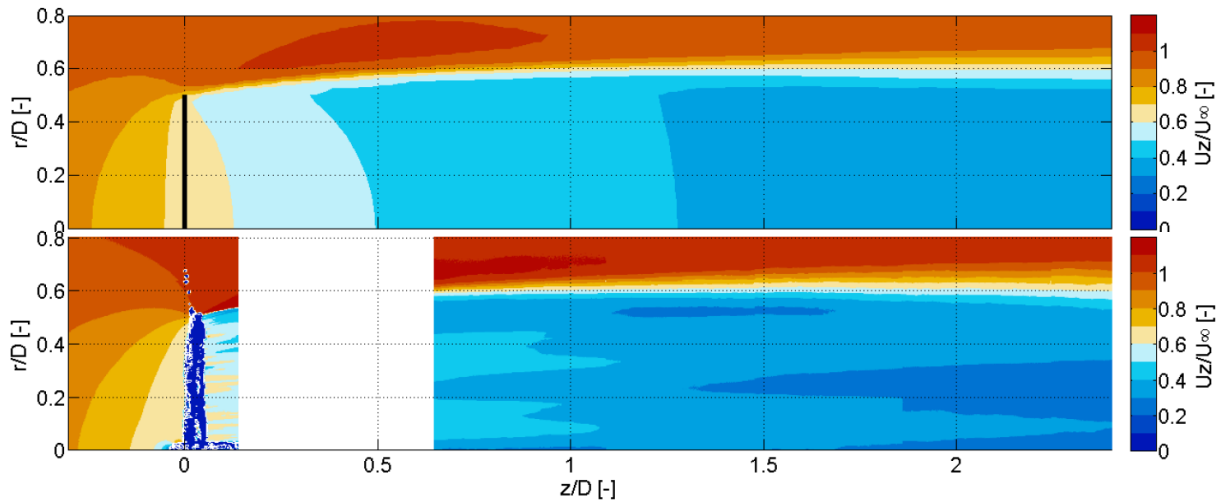
Figure 3. Average axial velocity profiles using a simulation of an AD at $C_T = 0.89$ (top) compared to a PIV experiment of an AD at $C_T = 0.93$ [27] (bottom).

*4.3. Comparison for the centerline velocity and thrust coefficients*

The left frame of figure 4 shows the centerline velocity for the Betz limit ($C_T = 0.89$) compared to a numerical potential flow solution from literature [23]. The results for the simulation with the VPM are given over a range of core sizes. A very good comparison between all results is visible up to 2 diameters downstream. Thereafter a wobble in the simulation results are apparent, but this is caused by a mismatch between the semi-infinite analytical vortex tube applied from 5 diameters onwards, as the theoretical wake expansion is not reached by the VPM. This causes the particles to collapse inbound in the radial direction (as was visualized in figure 2).

In the right frame of figure 4 the simulation results for a range of thrust coefficients is presented and set off against the axial induction factor a at the AD (blue circled dots). The parabola gives the theoretical relationship, while the dashed lines and red crossed dots indicate correction factors for highly-loaded rotors (Glauert, Burton, and Wilson) and empirical results (Lock) respectively [28]. For lower thrust values up to the Betz limit, the theoretical curve is closely approximated. For highly-loaded rotors ($C_T \geq 1$) the results obtained with the VPM deviate from theory and follow that of the correction factors and empirical results. It has to be mentioned though that it is difficult to define the axial induction factors for the highly-loaded results, as periodic shedding of the starting vortex is manifested. In this case, the axial induction factors are taken as underbounds, but at least the trend is clear.

5. Results and discussions of HAWT simulations with prescribed circulation from the MEXICO experiment

5.1. Inviscid simulation

Figure 5 shows the result for the axial velocity profile (top frame) and the vorticity profile (bottom frame) after 9 rotor rotations utilizing a VPM simulation with prescribed circulation from the MEXICO experiment. A chaotic flow pattern is distinguishable after 2 diameters downstream, which is the result of a turbulent region of highly stretched vortices. These thin and therefore very intense vortices make the numerical simulation unstable and beyond the currently demonstrated instance of time the particle geometry actually blows up.
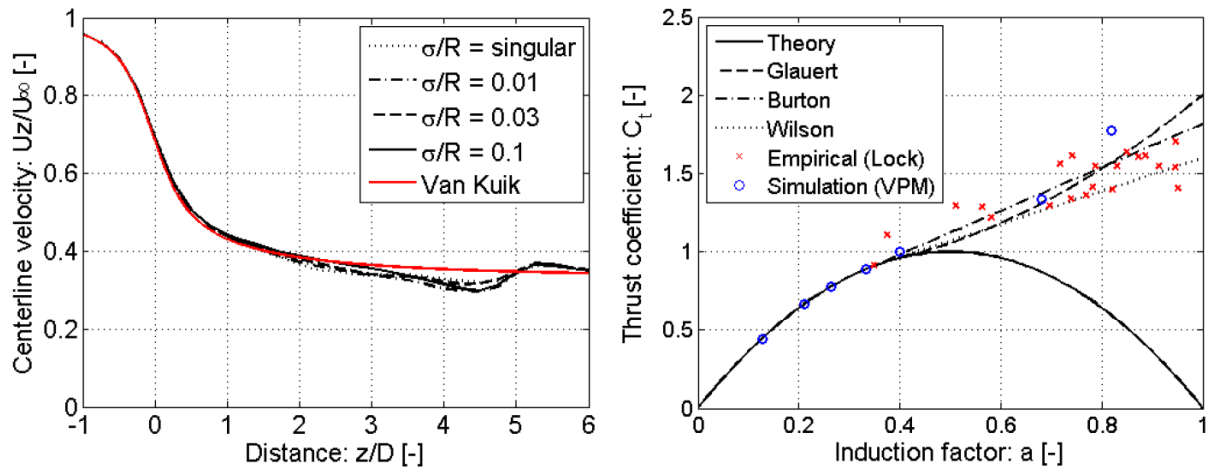
Figure 4. Axial velocity on the centerline (left), and a comparison of a range of thrust coefficients set off against the axial induction factor at the AD (right).
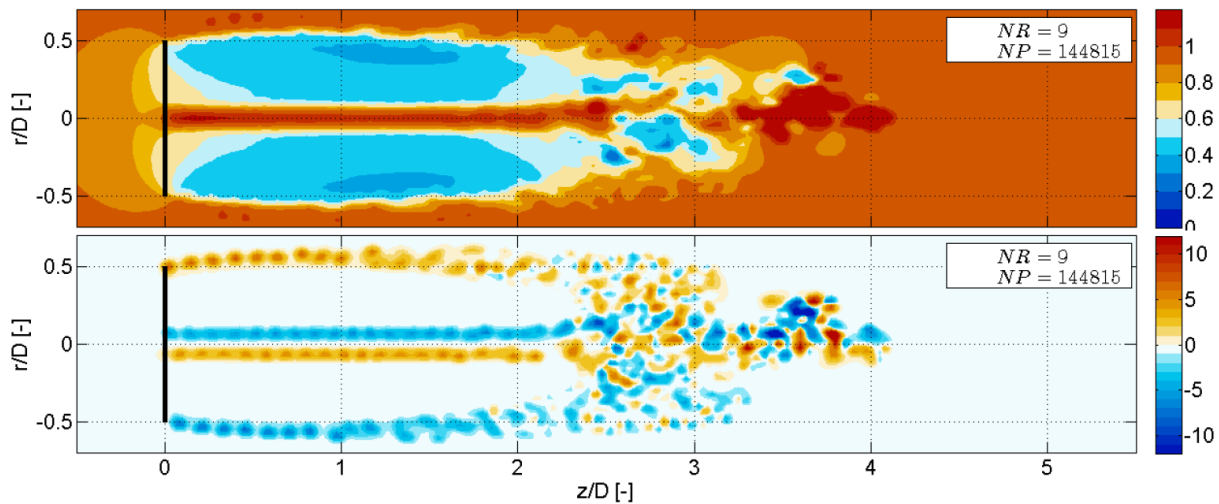
Figure 5. Instantaneous inviscid near-wake simulations of the MEXICO rotor. Shown are the axial velocity (top) and the vorticity (bottom). The classic stretching scheme is applied.

5.2. Simulation with a PSE-scheme applied for $Re = DU_\infty/\nu = 1.9 \cdot 10^4$

To counteract the formation of undesirably small vortex scales as demonstrated in figure 5, a Particle Strength Exchange (PSE) scheme is applied which transports vorticity out of local intense regions. In this way the uncontrolled growth of fine turbulent structures is successfully tempered (figure 6). Shown is the result after 12 rotations, at which point the simulation is still stable. Note also the amount of particles ($NP = 40483$) which is a lot less than for the result of figure 5 ($NP = 144815$), due to the fact that now no uncontrolled stretching is manifested; i.e. less particle splitting occurs. Note worthy are also the significant viscous dissipation of the root vortex, and the outer shear layer which remains intact for a prolonged amount of time due to the low Reynolds number.
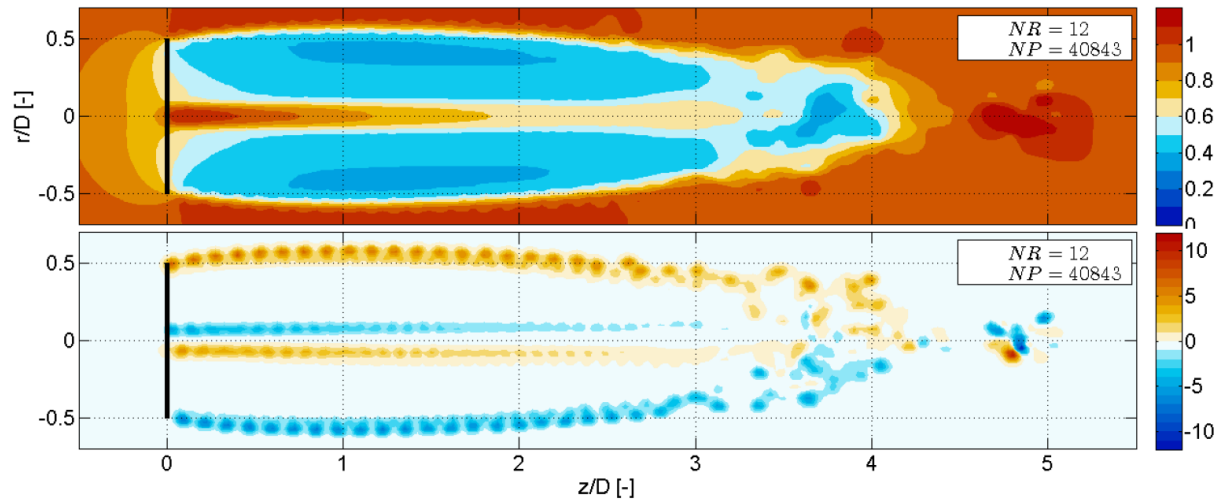
Figure 6. Near-wake simulations of the MEXICO rotor with a PSE-scheme implemented ($Re = DU_\infty/\nu = 1.9 \cdot 10^4$). Shown are the axial velocity (top) and the vorticity (bottom). The classic stretching scheme is applied.
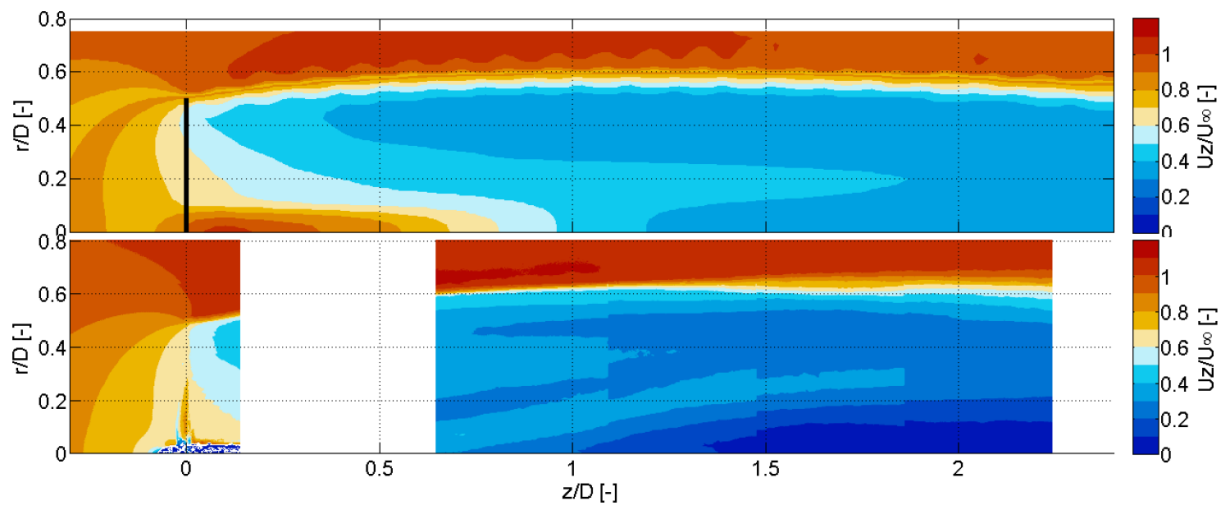
5.3. Comparison of the axial velocity with a 2-bladed PIV experiment

The axial velocity profile of a simulation of a 3-bladed HAWT with prescribed circulation (top frame) is compared to that of PIV results from another experiment utilizing a 2-bladed HAWT [27] ($TSR = 6.0$ and $C_T = 0.89$, bottom frame), see figure 7. Results in blank regions are not captured due to limitations in the PIV setup. The simulation result is instantaneous, while the PIV result is averaged over time. For the simulation a transpose stretching scheme is applied for a better maintaining of numerical stability, and a small relaxation [19] of $f = 0.02$ for counteracting numerical divergence to some extent.

Although the results represent different turbines under slightly different conditions, the wake deficit profile is qualitatively speaking comparable. several tendencies can be extracted that typify the VPM simulation, though. Both simulations show a break-up of the root vortex which is visible as an increased wake deficit around the centerline, but the nature of this phenomenon is different for both cases. For the experiment (bottom frame) this is caused by the presence of the nacelle, which results in flow blockage and added wake turbulence. The simulation (top frame) does not model the nacelle, but the root vortex breaks down due to manifestation of numerical divergence after 0.5 rotor diameters downstream. Moreover, the experiment (bottom frame) produces a sharp shear layer and a rapid shear layer expansion beyond 1.5 diameters downstream due to leapfrogging of the tip vortices. The simulation (top frame) needs to satisfy the overlapping condition, which smears out the shear layer vorticity right from the onset at the rotor. As a sharp shear layer is required for triggering the Kelvin-Helmholtz instability, the shear layer expansion is therefore oppressed.

5.4. Comparison of the axial velocity with the MEXICO experiment

The final comparison that will be discussed in this paper is that between some simulations using the VPM and windtunnel results of the real MEXICO experiment. In figure 8, the axial and radial velocity over the near-wake is presented at two radial positions, at midspan where $r/R = 0.52$ (left frame) and near the tip where $r/R = 0.91$ (right frame). The circles and squares denote the empirical axial and radial results respectively, while the lines give the simulation results for three different cases (inviscid classic scheme, classic scheme with PSE, and transpose scheme with PSE applied).

Figure 7. Comparison between a simulation utilizing a transpose stretching scheme and PSE applied ($Re = DU_\infty/\nu = 1.9 \cdot 10^4$), and a PIV experiment of a 2-bladed turbine at $TSR = 6.0$ and the Betz limit ($C_T = 0.89$) for the axial velocity profile over the near-wake.

The discrepancy between the empirical and simulation results between the rotor and 0.5 diameter downstream is caused by laser reflections of the PIV setup employed. Outside of this region, the results compare very well, although the axial velocity is slightly higher further downstream (smaller wake deficit) for the simulation results as the wake expansion has not reached full expansion yet at this instance in time. The axial wake deficit downstream is a bit larger when PSE and the transpose scheme are applied, as this results in a delay of the Kelvin-Helmholtz instability.
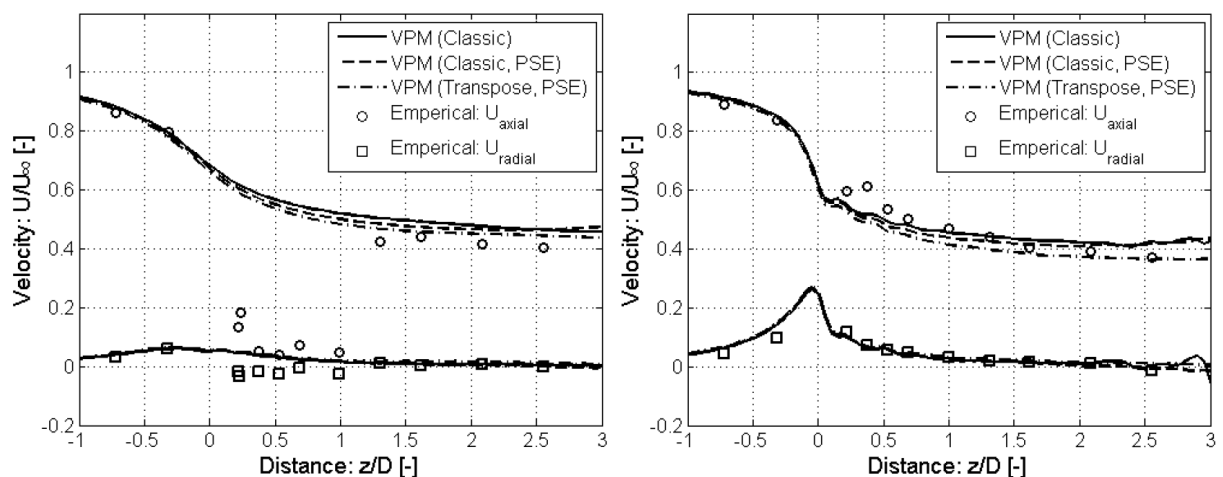
Figure 8. The axial and radial velocity in the near-wake for the radial blade positions of $r/R = 0.52$ (left) and $r/R = 0.91$ (right). The empirical results are from literature [26].

6. Conclusions

The application of a Vortex Particle Method (VPM) for modelling the near-wake of an Actuator Disc (AD) and a 3-bladed Horizontal Axis Wind Turbine (HAWT) has been explored. The VPM

was designed to simulate the 3-dimensional flow in a Lagrangian framework and able to run in parallel on a cluster of CPUs. To accelerate the simulation even further, a coupling to a Fast Multipole Method (FMM) has been achieved which optimally brings down the computational effort from N^2 to $N \log N$.

Simulations with the axisymmetric AD resulted in the correct behaviour of distinctive quantities such as wake expansion, axial velocity deficit, and induction factor at the AD, which have been validated against several theoretical, numerical, and experimental results from literature. Also shear layer expansion has been achieved beyond 1 diameter downstream as the Kelvin-Helmholtz instability was triggered due to the inherent numerical round-off errors involved. However, a Particle Image Velocimetry (PIV) experiment showed an immediate shear layer expansion right from the onset at the AD as the shear layer of this experiment was initially sharp, while a smooth shear layer was initiated with the VPM to guarantee the vital particle overlap.

The simulations involving a 3-bladed turbine with prescribed circulation from the MEXICO experiment allowed a fully 3-dimensional flow computation. The formation of highly-stretched small scale turbulence was visible beyond 2 diameters downstream, which made the simulation become unstable. To mitigate vorticity from these locally intense regions, a PSE scheme to model viscous diffusion has been successfully applied. wake simulations have been run beyond 4 diameters downstream at which point stability was still maintained. Close comparisons with results from the real MEXICO experiment have been obtained for the axial and radial velocity over the near wake. A comparison with a PIV experiment of a 2-bladed turbine indicated a similar wake expansion and axial velocity deficit, but the shear layer expansion of the VPM simulations was to a great extent suppressed by the large core size and low Reynolds number of the PSE scheme applied. Moreover, the PIV results showed a large influence of the shadowing effect of the generator, which was not modelled with the VPM.

Simulations have been run with both the classic scheme and the transpose scheme for vortex stretching. Where the first proved to be more accurate as it inherently maintains the divergence-free properties (vortices remain linked), the latter showed to result in more stable simulations although the divergence especially in the root vortex was a major issue. Methods that suppress the divergence are therefore necessary when the transpose scheme is applied.

The present work showed that accurate 3-dimensional simulations of the near-wake of a HAWT are achievable with a Lagrangian VPM, even on a single CPU or utilizing a small cluster. The smoothing of the particle field, and treatment of divergence and flow complexities evolving from intense vortex stretching have proved to be essential both for the accuracy and stability of the method.

References

[1] Sørensen J N 2011 Aerodynamic aspects of wind energy conversion *Annu. Rev. Fluid Mech.* **43** 427-448
[2] Chatelain P, Backaert S, Winckelmans G and Kern S 2013 Large eddy simulation of wind turbine wakes *Flow, Turbul. Combust.* **91(3)** 587-605.
[3] Backaert S, Chatelain P and Winckelmans G 2015 Vortex Particle-Mesh with immersed lifting lines for aerospace and wind engineering *Procedia IUTAM* **18** 1-7
[4] Voutsinas S G, Belessis M A and Rados K G 1995 Investigation of the yawed operation of wind turbines by means of a vortex particle method Agard Conference Proceedings p 11
[5] Yokota R, Sheel T K and Obi S 2007 Calculation of isotropic turbulence using a pure Lagrangian vortex method *J. Comp. Phys.* **226(2)** 1589-1606
[6] Yokota R, Narumi T, Sakamaki R, Kameoka S, Obi S and Yasuoka K 2009 Fast multipole methods on a cluster of GPUs for the meshless simulation of turbulence *Comput. Phys. Commun.* **180(11)** 2066-2078
[7] Yokota R and Barba L A 2011 Comparing the treecode with FMM on GPUs for vortex particle simulations of a leapfrogging vortex ring *Comput. Fluids* **45(1)** 155-161
[8] Yokota R and Barba L A 2013 FMM-based vortex method for simulation of isotropic turbulence on GPUs, compared with a spectral method *Comput. Fluids* **80** 17-27

[9] Hu Q, Syal M, Gumerov N A, Duraiswami R and Leishman J G 2011 Towards improved aeromechanics simulations using recent advancements in scientific computing *Proc. 67th Annual Forum of the American Helicopter Society*

[10] Hu Q, Gumerov N A, Yokota R, Barba L and Duraiswami R 2012 Scalable fast multipole methods for vortex element methods *High Performance Computing, Networking, Storary and Analysis (SCC), 2012 SC Companion* p 1408

[11] Berdowski T 2015 3D Lagrangian VPM-FMM for modelling the near wake of a HAWT *(Master's thesis)*

[12] Sbalzarini I F, Walther J H, Bergdorf M, Hieber S E, Kotsalis E M and Koumoutsakos P 2006 PPM   A highly efficient parallel particle-mesh library for the simulation of continuum systems. *J. Comput. Phys.* **215(2)** 566-588

[13] Cottet G H and Koumoutsakos P D 2000 Vortex methods: theory and practice *Cambridge university press*

[14] Winckelmans G S 1989 Topics in vortex methods for the computation of three- and two-dimensional incompressible unsteady flows *Dissertation (Ph.D.), California Institute of Technology*

[15] Chorin A J 1973 Numerical study of slightly viscous flow *J. Fluid Mech.* **57(04)** 785-796

[16] Leonard A 1980 Vortex methods for flow simulation *J. Comput. Phys.* **37(3)** 289-335

[17] Rossi L F 1996 Resurrecting core spreading vortex methods: A new scheme that is both deterministic and convergent *SIAM J. Sci. Comput.* **17(2)** 370-397

[18] Degond P and Mas-Gallic S 1989 The weighted particle method for convection-diffusion equations. I. The case of an isotropic viscosity *Math. Comp.* **53(188)** 485-507.

[19] Pedrizzetti G 1992 Insight into singular vortex flows *Fluid Dynamics Research* **10(2)** 101-115

[20] Barnes J and Hut P 1986 A hierarchical O (N log N) force-calculation algorithm *nature* **324(6096)** 446-449

[21] Greengard L and Rokhlin V 1987 A fast algorithm for particle simulations *J. Comput. Phys.* **73(2)** 325-348

[22] Berdowski T, Walther J and Ferreira C 2016 Derivation and analysis of the analytical velocity and vortex stretching expressions for an $\mathcal{O}(N \log N)$-FMM *Manuscript in preparation*

[23] Kuik G A M and Lignarolo L E M 2015 Potential flow solutions for energy extracting actuator disc flows *Wind Energy*

[24] Yu W, Ferreira C, and Van Kuik G A M 2016 Analytical actuator disk solution for unsteady and/or non-uniform loading *34th Wind Energy Symposium, San Diego, USA*

[25] Micallef D, van Bussel G, Ferreira C and Sant T 2013 An investigation of radial velocities for a horizontal axis wind turbine in axial and yawed flows *Wind Energy* **16(4)** 529-544

[26] Nilsson K, Shen W Z, Sorensen J N, Breton S P and Ivanell S 2015 Validation of the actuator line method using near wake measurements of the mexico rotor *Wind Energy* **18(3)** 499-514

[27] Lignarolo L E M, Ragni D, Krishnaswami C, Chen Q, Ferreira C, van Bussel G J W and Chen Q 2014 Experimental analysis of the wake of a horizontal-axis windturbine model *Renew. Energy* **70** 31-46

[28] Buhl M L 2005 A new empirical relationship between thrust coefficient and induction factor for the turbulent windmill state. *National Renewable Energy Laboratory*